Thermal Exchange-Correlation Functionals: Capturing Quantum Electron Behavior in Warm, Dense Plasmas

Valentin V. Karasiev,[1,*] S. X. Hu,[1,2,3] Katerina P. Hilleke,[1]
Ammar A. Ellaboudy,[1,2] Deyan I. Mihaylov,[1] and S.B. Trickey[4]

[1] *Laboratory for Laser Energetics, University of Rochester, Rochester, NY 14623, USA*
[2] *Department of Physics and Astronomy, University of Rochester, Rochester, NY 14627, USA*
[3] *Department of Mechanical Engineering, University of Rochester, Rochester, NY 14627, USA*
[4] *Quantum Theory Project, Departments of Physics and of Chemistry, University of Florida, Gainesville, FL 32611*

(Dated: 08 Dec. 2025)

We summarize and give perspective upon recent progress in developing non-empirical constraint-based thermal (i.e. free energy) exchange-correlation (XC) density functionals essential for accurate description of the quantum behavior of electrons in warm, dense plasmas. After delineating the critical role of ground-state functionals for zero-temperature, time-dependent DFT, we outline the underpinnings of local density approximation (LDA), generalized gradient approximation (GGA), and meta-GGA XC free-energy functionals. Two basic thermalization principles for upgrading ground-state XC functionals to successful thermal ones are emphasized. Then we turn to a long-standing challenge, assessment of the accuracy of well-founded functionals. Unlike the ground state, there are few exact results for large T and P. An exception is path integral Monte Carlo (PIMC) data for dense H/D and He plasmas. For those, we did *ab-initio* molecular dynamics (AIMD) simulations under selected thermodynamic conditions employing five thermal XC functionals: two approximate thermal GGAs, fully-thermal GGA, an approximate meta-GGA, and fully-thermal meta-GGA. Comparisons with the PIMC data show that functionals thermalized by augmenting a non-thermal functional with a lower-level thermal contribution are inferior to functionals with thermal XC and spatial inhomogeneity effects taken into account at the same level of refinement. We believe this and similar evidence should be convincing to the high-energy density physics community of the necessity of use of proper thermal XC functionals in simulation studies of finite-temperature quantum effects in warm, dense plasmas.

I. INTRODUCTION

The state of the art for predictive quantum calculation of static or quasi-static properties of materials under extreme conditions (e.g. non-ideal plasmas, planetary interiors, compression pathways to ICF, warm dense matter (WDM)) is *ab initio* molecular dynamics (AIMD) driven by Mermin-Kohn-Sham (MKS) finite-temperature (i.e. free-energy) density functional theory (DFT) treatment of the electrons [1, 2]. In parallel with ground-state DFT, MKS-DFT maps the fully interacting many-electron system onto an auxiliary non-interacting system in which all many-body quantum effects (i.e. exchange and correlation) are subsumed in an exchange-correlation (XC) density functional. Though its formal properties are known, there is no explicit exact form. Thus, the accuracy of MKS-DFT calculations hinges on the accuracy of a XC-functional approximation.

For cases in which a quasi-static treatment is inappropriate (for example, system relaxation time of the same scale as some characteristic oscillation, $t_{relax} \lessapprox t_{vib}$), a dynamical treatment is needed. An obvious choice is time-dependent DFT (tD-DFT). A key challenge for such calculations is a sufficiently accurate time-dependent, thermal exchange-correlation (XC) kernel [3]. For that it is a common procedure, even at $T = 0$, to use the adiabatic approximation $\mathcal{F}_{xc}[n;T,t] \approx \mathcal{F}_{xc}[n(t,T),T(t)]$ with the latter functional being the *time-independent* $\mathcal{F}_{xc}$ evolved at the current values of n and T at time t. Here we are not concerned with the limits or validity of the adiabatic approximation. Rather we focus on the sometimes underappreciated implication, namely the importance of the time-independent $\mathcal{F}_{xc}$ for dynamical problems. To reinforce the point, one also notes that even in the case of a genuine dynamical finite-temperature kernel, the zero-frequency limit must be $\mathcal{F}_{xc}$.

Thus the accuracy of both tD-DFT and finite-T quasi-static MKS-DFT predictions depends crucially on the accuracy of $\mathcal{F}_{xc}$ approximations. That is the issue addressed here. A common approach in AIMD calculations has been to use the ground-state approximation (GSA). In it, the XC free-energy is evaluated using a ground-state temperature-independent functional: $\mathcal{F}_{xc}[n;T] \approx E_{xc}[n]$. The approach lacks explicit XC thermal effects (it may have an implicit T-dependence via the minimizing density or, also, the kinetic energy density), and completely misses the XC entropy. The GSA therefore is the crudest approximation. It can be unreliable especially in the warm-dense regime, with errors up to 20% in predicted pressure and energy relative to experimental values [4–10].

That comparison introduces another challenge to $\mathcal{F}_{xc}$ development, namely the relative paucity of high-

* vkarasev@lle.rochester.edu

accuracy calculated reference data. For ground state E_{xc}, there is a considerable inventory of high-accuracy many-fermion calculations on small and medium-sized molecules The literature is too extensive to cite thoroughly but see Refs. 11, 12 and references therein for recent examples. However, for large, periodic systems, especially those at relatively high T and P, there are very few exact results. One partial exception is a calculation on the Hubbard dimer [13], but even its authors characterize the study as providing only "... a first glimpse at the behaviors of correlation energy components as a function of temperature ... ". Another exception to the general paucity of calibration data is path integral Monte Carlo results for dense H/D and He plasmas [14–17]. Those are targets in this work.

The development of XC free-energy functionals can be classified by the level of theoretical refinement as rungs of the finite-T analog of the ground-state Perdew-Schmidt ladder [18] shown in Fig. 1. The first rung is the local density approximation (LDA) which depends on electron density (n) and temperature (T). That rung is occupied by the Karasiev-Sjostrom-Dufty-Trickey (KSDT) functional developed in Ref. [19] (see Ref. [5] for the corrected version, corrKSDT) and the Groth-Dornheim-Sjostrom-Malone-Foulkes-Bonitz (GDSMFB) functional [20]. It is a refinement of KSDT XC form and methodology to match improved Monte Carlo data for the homogeneous electron gas (HEG) at finite-T and low $r_s = (3/4\pi n)^{1/3}$ (the Wigner-Seitz radius) [21, 22].

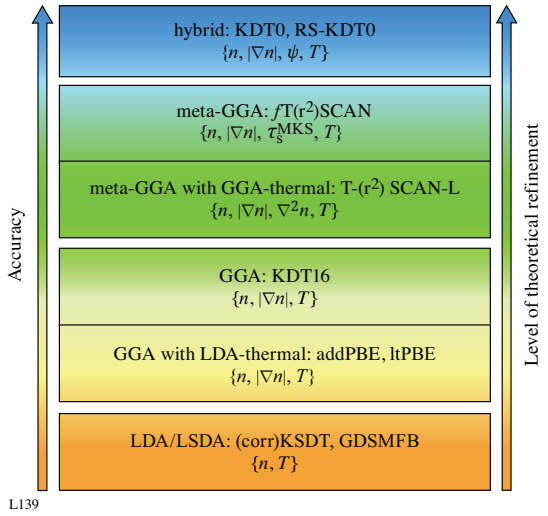

FIG. 1. The ladder of temperature-dependent XC functionals. LDA: (corr)KSDT [5, 19] and GDSMFB [20]. GGA: KDT16 [5], addPBE [23] and ltPBE [24]. Meta-GGA: T-(r^2)SCAN-L [8] and fTSCAN [9]. Hybrid: KDT0 [25] and RS-KDT0 [26].

The fully thermal GGA (the second rung), with added dependence on the electron density gradient, is the Karasiev-Dufty-Trickey (KDT16) [5]. There also are two approximate GGA-level functionals with additive and multiplicative LDA-level thermal corrections respectively, termed the additive Perdew-Burke-Ernzerhof (addPBE) [23] and locally thermal PBE (ltPBE) [24].

Development of the third, meta-GGA rung is represented by two approaches: (i) a simple approximate scheme which uses a universal additive GGA-level thermal correction applied to either the ground-state deorbitalized, strongly constrained, and appropriately normed (SCAN-L) or to the deorbitalized version of the regularized-restored r^{2}SCAN-L functional, called T-SCAN-L and T-r^{2}SCAN-L [8], and (ii) the fully thermal meta-GGA framework developed in Ref. [9] and utilized to construct fTSCAN. Compared to GGA functionals, deorbitalized meta-GGA XC functionals, both ground-state and free-energy, have added dependence on the electron density Laplacian as well as n and $|\nabla n|$. The parent ground-state meta-GGA depends instead on the non-interacting kinetic energy density (KED), $\tau_s^{KS}(\{\psi\})$, rather than $\nabla^2 n$. Thus, the fully thermal fTSCAN depends on the Mermin-Kohn-Sham (MKS) orbitals via the finite-T non-interacting kinetic energy density (KED), $\tau_s^{MKS}(\{\psi\}, T)$, in addition to n and $|\nabla n|$.

Functionals on the first three rungs are semi-local or one-point density functionals. The fourth rung corresponds to hybrid XC functionals. Those depend explicitly on the KS or MKS orbitals via inclusion of some fraction of non-local Fock exchange. For $T > 0$, two such exist, the global hybrid KDT0 [25], and the range-separated RS-KDT0 [26] both developed by the Theoretical High-Energy-Density Physics Group at University of Rochester. These finite-temperature hybrid XC-functionals have delivered better performance (compared to lower-rung functionals) in predicting band-gap closing behavior in warm-dense matter.

The next section gives essential details about formulation of free-energy XC functionals at each rung. Section III compares the performance of such thermal XC functionals in predicting properties of materials in warm-dense and near-ambient regimes. A summary is given in Sec. IV.

II. CONSTRUCTION OF EXCHANGE-CORRELATION FREE-ENERGY FUNCTIONALS

We turn to a concise description of thermalization procedures for upgrading well-founded ground-state XC functionals into free-energy XC functionals at each rung of the Perdew-Schmidt complexity ladder. Much of this involves thermalization of functional variables. Before going into details we emphasize two comprehensive principles of the thermalization that apply directly to free-energy functional development at all rungs.

• Preserve the zero-T limit: as $T \to 0$, the thermalized XC functional must reduce to a specified, well-founded ground-state functional. Correspondingly, finite-T LDA must reduce very closely to a reliable zero-T HEG parametrization. The obvious objective is to preserve all zero-T exact constraints and norms used in the ground-

state XC construction.

• Enforce important exact finite-T constraints, for example, correct uniform density scaling [27], consistency with the finite-T gradient expansion for weakly inhomogeneous density at all T for X and C at least through second order (in the case of GGA and meta-GGA) (see references in Ref. [5]), and the correct high-T limit.

A. Local density approximation

The KSDT parametrization of restricted path integral Monte Carlo (RPIMC) data for the finite T HEG [21] was the first accurate analytical representation for the HEG XC free energy. It is the XC free-energy LSDA counterpart of the celebrated Perdew-Zunger [28] ground-state LDA parametrization of the Ceperley-Alder [29] HEG data. The available finite-T RPIMC HEG data was the interacting system kinetic energy per particle, τ, and potential energy per particle, $u_{\rm ee}$ From those, the XC free energy per particle, $f_{xc} = \varepsilon_{\rm xc} - T\sigma_{\rm xc}$ had to be extracted and fitted. Various Maxwell relations provide four distinct routes for doing that. Evaluation of all four led KSDT to proceed as follows.

First, $\varepsilon_{\rm xc}$, the XC internal energy (per particle) is the difference of the interacting and non-interacting system internal energies, $\varepsilon_{\rm xc} = \tau + u_{\rm ee} - \tau_{\rm s}$, where $\tau_{\rm s}$ is the non-interacting HEG kinetic energy per particle at $T > 0$ [30, 31]. Second, there is the thermodynamic definition of the entropy per particle

$$\sigma_{\rm xc}(r_{\rm s},t) = -\frac{t}{T}\frac{\partial f_{\rm xc}(r_{\rm s},t)}{\partial t}\Big|_{r_{\rm s}} . \qquad (1)$$

Invoking it gives a differential equation for $f_{\rm xc}$ from $\varepsilon_{\rm xc}$

$$f_{\rm xc}(r_{\rm s},t) - t\frac{\partial f_{\rm xc}(r_{\rm s},t)}{\partial t}\Big|_{r_{\rm s}} = \varepsilon_{\rm xc}(r_{\rm s},t)\,, \qquad (2)$$

where here $t = T/T_{\rm F}$ [$T_{\rm F} = (1/2)(9\pi/4)^{2/3} r_{\rm s}^{-2}$] is the reduced temperature.

Matching the solution of this differential equation to the RPIMC data requires design of a suitable analytical form of $f_{\rm xc}$. For the spin-unpolarized case, KSDT extended a Padé approximant [32] form given by Ichimaru *et al.*[33] in the $r_{\rm s}^{1/2}$ variable with t-dependent coefficients

$$f_{\rm xc}^{\rm LDA}(r_{\rm s},t) = -\frac{1}{r_{\rm s}}\frac{a(t) + b(t) r_{\rm s}^{1/2} + c(t) r_{\rm s}}{1 + d(t) r_{\rm s}^{1/2} + e(t) r_{\rm s}} . \qquad (3)$$

The coefficient functions are too complicated to be worth displaying. The correct high-density (small-$r_{\rm s}$) and small Γ (Coulomb coupling parameter) limits for $f_{\rm xc}$ were incorporated by constraints on $a(t)$, while the correct high-T limit is built in via constraint on one of the coefficients in $b(t)$. Then Eq. (2) was solved by minimizing the difference between $\varepsilon_{\rm xc}$ evaluated from Eq. (3) and the reference Monte Carlo data via variation of the parameters in the coefficient functions $b(t) - e(t)$ (see Ref. [19]).

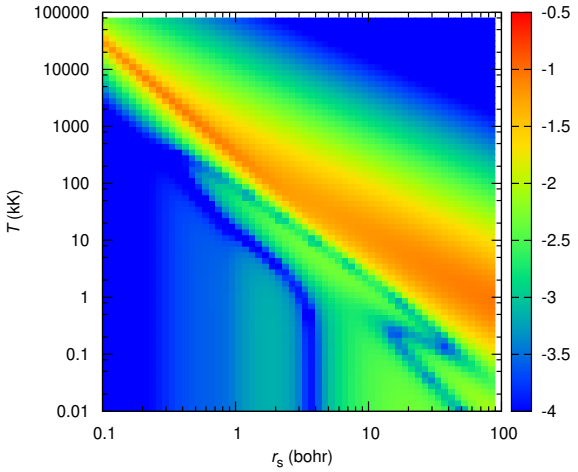

FIG. 2. Color map in the $(r_{\rm s}, T)$ plane of relative importance of explicit T-dependence in the HEG XC free-energy functional measured as the upper bound $\mathcal{R}$ (see text for definition) (reproduced from Ref. [4]).

The corrected KSDT version (corrKSDT) [5] utilized improved quantum Monte Carlo data [34]. Because those data were for u_{ee}, a different thermodynamic route had to be used. The refit also corrected an almost inconsequential $T = 0$ data fitting error and a cosmetic negative entropy at very large r_s. It turned out that a seeming flaw in KSDT at low t and $r_s = 1.0$ actually was a flaw in the original data. Further details on the fully spin polarized case and a T-dependent interpolation for intermediate polarizations can be found in Ref. [19].

The GDSMFB parametrization [20] (contemporaneous with corrKSDT) used their QMC data, the same $F_{\rm xc}$ representation Eq. (3), the same thermodynamic route as corrKSDT, and the KSDT T-dependent interpolation for intermediate polarizations. The equivalence of these two representations and their limitations are discussed in Ref. [35].

Fig. 2 shows the relative magnitude of XC thermal effects in the HEG as a function of $r_{\rm s}$ and T in terms of $\mathcal{R} := \log_{10}(|f_{\rm xc}^{\rm LDA}(r_{\rm s},T) - \varepsilon_{\rm xc}^{\rm LDA}(r_{\rm s})|/[|f_{\rm s}^{\rm LDA}(r_{\rm s},T)| + |\varepsilon_{\rm xc}^{\rm LDA}(r_{\rm s})|])$. The denominator is an upper-bound to the HEG total free-energy per particle since it is the sum of absolute values of the non-interacting free-energy, $f_{\rm s}^{\rm LDA}$ and the ground-state LDA XC energy per particle, $\varepsilon_{\rm xc}^{\rm LDA}$. Thus $\mathcal{R}$ deliberately underestimates the magnitude of XC thermal effects. Those clearly are negligible at low-T (except perhaps at very large $r_{\rm s}$, *i.e.*, very low density), as expected. That also is true for very high-T because the total free-energy in that regime is dominated by the non-interacting contribution, hence essentially is independent of the XC approximation. The nearly diagonal orange-yellow band indicates a range of thermodynamic conditions in which finite-T XC effects may be important.

These HEG results can serve as a rough indicator of

regions of thermal XC importance in real inhomogeneous systems. In terms of the reduced temperature t, the orange-yellow band converts into a near-horizontal one indicating that the thermal effects may be important for t above a few tenths and up to t between 1 and 10, depending on the electron density (further details are in Ref. 6).

B. GGA: fully thermalized

Development of the GGA XC free-energy is based on analysis of the finite-T second-order gradient expansions for X and C, the ensuing definition of dimensionless reduced density gradient variables with explicit T-dependence for X and C, and construction of a functional with the same structure as in a suitably chosen ground-state GGAs (which will be the $T \to 0$ limit of the free-energy version), namely an exchange enhancement factor and correlation free-energy per particle.

That structure implicates the corrKSDT thermal LDA XC parametrization Eq. (3), partitioned into X and C terms, as a key ingredient for successful construction of a thermal GGA. The LDA X free-energy per particle has the factorized form [36]

$$f_{\rm x}^{\rm LDA}(n,t) = \varepsilon_{\rm x}^{\rm LDA}(n)\widetilde{A}_{\rm x}(t)\,, \tag{4}$$

$$\varepsilon_{\rm x}^{\rm LDA}(n) = -\frac{3}{4}\Big(\frac{3}{\pi}\Big)^{1/3} n^{4/3}\,, \tag{5}$$

$$\widetilde{A}_{\rm x}(t) = \frac{t^2}{2}\int_{-\infty}^{(\beta\mu)} I_{-1/2}^2(\eta)d\eta\,. \tag{6}$$

Here $\beta = (k_{\rm B}T)^{-1}$, I_α is the Fermi-Dirac (FD) integral [37], and μ is the chemical potential defined by the density as $n = \sqrt{2}I_{1/2}(\beta\mu)/(\pi^2\beta^{3/2})$. The LDA correlation free-energy per particle then is defined in terms of the corrKSDT LDA parametrization as $f_{\rm c}^{\rm LDA}(n,t) = f_{\rm xc}^{\rm LDA}(n,t) - f_{\rm x}^{\rm LDA}(n,t)$.

The central ingredient for GGA development is the second-order term in the finite-T gradient expansion [23, 38–42]

$$f_{\rm xc}^{(2)}(n,\nabla n,T) = \tfrac{1}{2}g_{\rm xc}^{(2)}(n,T)\frac{|\nabla n(\mathbf{r})|^2}{n(\mathbf{r})}\,. \tag{7}$$

It can be separated into X and C contributions, $f_{\rm xc}^{(2)} = f_{\rm x}^{(2)} + f_{\rm c}^{(2)}$, with the X term being

$$f_{\rm x}^{(2)}(n,\nabla n,T) = f_{\rm x}^{\rm LDA}(n,{\rm T})\frac{8}{81}\Big[\frac{\widetilde{B}_{\rm x}(t)}{\widetilde{A}_{\rm x}(t)}s^2(n,\nabla n)\Big]\,, \tag{8}$$

where $s := |\nabla n|/2(3\pi^2)^{1/3}n^{4/3}$ (the dimensionless reduced density gradient used in ground-state GGA functionals), and

$$\widetilde{B}_{\rm x}(\eta) = \frac{3^{4/3}}{2^{4/3}}I_{1/2}^{4/3}(\eta)\Big[\Big(\frac{I'_{-1/2}(\eta)}{I_{-1/2}(\eta)}\Big)^2 - 3\frac{I''_{-1/2}(\eta)}{I_{-1/2}(\eta)}\Big]\,. \tag{9}$$

Primes denote derivatives with respect to the argument. The bracketed term in Eq. (8) defines the explicitly T-dependent dimensionless reduced density gradient for the X free energy

$$s_{2\rm x}(n,\nabla n,T) \equiv s^2(n,\nabla n)\frac{\widetilde{B}_{\rm x}(t)}{\widetilde{A}_{\rm x}(t)}\,. \tag{10}$$

The second-order correlation term, $f_{\rm c}^{(2)}$, is proportional to $n^{1/3}s^2\widetilde{B}_{\rm c}(r_{\rm s},t) \propto \mathcal{Q}^2\widetilde{B}_{\rm c}(r_{\rm s},t)$, where $\mathcal{Q}(n,\nabla n) = |\nabla n|/2k_{\rm s}n$ is the relevant ground-state variable and $k_{\rm s} = 2(3n/\pi)^{1/6}$. This allows one to define the T-dependent reduced density gradient for correlation as

$$\mathcal{Q}_{\rm c}(n,\nabla n,T) = \mathcal{Q}(n,\nabla n)\sqrt{\widetilde{B}_{\rm c}(r_{\rm s},t)}\,. \tag{11}$$

The gradient correction coefficient $g_{\rm xc}^{(2)}(n,T)$ was evaluated numerically in Ref. 23 by use of a relation to the static local field correction [43, 44] and finite-T quantum Monte-Carlo data[21]. The numerical data for $g_{\rm xc}^{(2)}$ in combination with Eqs. (7) and (8) enables numerical evaluation of the function $\widetilde{B}_{\rm c}(r_{\rm s},t)$. Refs. 5, 45 gave accurate analytic fits (including proper asymptotic behaviors) for the functions $\widetilde{A}_{\rm x}(t)$ and $\widetilde{B}_{\rm x}(t)$ defined as combinations of FD integrals through Eqs. (6) and (9) respectively, and the function $\widetilde{B}_{\rm c}(n,t)$ defined by numerical data on a $(r_{\rm s},t)$ grid.

With that and use of the T-dependent reduced density gradients, $s_{2\rm x}$ and $\mathcal{Q}_{\rm c}$, Eqs. (10), (11) respectively, the fully thermal GGA X enhancement factor is

$$\mathcal{F}_{\rm x}^{\rm GGA}[n,T] = \int n f_{\rm x}^{\rm LDA}(n,t)F_{\rm x}(s_{2\rm x}){\rm d}\mathbf{r}\,, \tag{12}$$

and the C free-energy per particle is

$$\mathcal{F}_{\rm c}^{\rm GGA}[n,T] = \int n f_{\rm c}^{\rm GGA}(n,t,\mathcal{Q}_{\rm c}){\rm d}\mathbf{r}\,. \tag{13}$$

In these, $F(s_{2\rm x})$ and $f_{\rm c}^{\rm GGA}(n,t,q_{\rm c})$ for the spin unpolarized case are defined as

$$F_{\rm x}(s_{2\rm x}) = 1 + \frac{\nu_{\rm x}s_{2\rm x}}{1+a_G|s_{2\rm x}|}\,, \tag{14}$$

with $\nu_{\rm x} = 0.21951$, $a_G = \nu_{\rm x}/(F_{\rm x,max}-1)$, $F_{\rm x,max} = 1.804$, and

$$f_{\rm c}^{\rm GGA}(n,t,\mathcal{Q}_{\rm c}) = f_{\rm c}^{\rm LDA}(n,t) + H\Big(f_{\rm c}^{\rm LDA},\mathcal{Q}_{\rm c}\Big)\,, \tag{15}$$

and H is the PBE correlation function defined in Ref. 46 for the spin unpolarized case. Equations (12)-(15) define the fully thermal KDT16 GGA, $F_{\rm xc}^{\rm KDT16}[n,T] \equiv F_{\rm x}^{\rm GGA}[n,T] + F_{\rm c}^{\rm GGA}[n,T]$.

To our knowledge KDT16 is the only published fully thermal GGA. By construction it obeys important constraints. First, in the zero-T limit it reduces to being very close to the ground-state PBE functional,

$\lim_{T\to 0} \mathcal{F}_{\rm xc}^{\rm KDT16}[n,T] \approx E_{\rm xc}^{\rm PBE}[n]$, hence it inherits all the main properties of PBE including local satisfaction of the zero-T Lieb-Oxford bound [47]. Second, in the slowly-varying limit, KDT16 recovers the second-order finite-T gradient expansion. That seems to be the most important requisite for an accurate GGA XC free-energy functional. Third, the KDT16 X free-energy scales correctly, $\mathcal{F}_{\rm x}^{\rm GGA}[n_\lambda,T] = \lambda \mathcal{F}_{\rm x}^{\rm GGA}[n,T/\lambda^2]$, with $n_\lambda(\mathbf{r}) = \lambda^3 n(\lambda \mathbf{r})$, see Refs. 27, 48. Fourth, KDT16 reduces properly to the corrKSDT LDA in the high-T limit.

C. GGA: LDA-thermal corrected

Two simple approximations based on a ground-state GGA with an LDA-level thermal correction have appeared. The first (called "addPBE") [23] takes the "subtract and add" form with respect to the ground-state PBE functional to yield the XC free-energy per particle as

$$f_{\rm xc}^{\rm addPBE}(n,\nabla n,t) = \varepsilon_{\rm xc}^{\rm PBE}(n,\nabla n) - \varepsilon_{\rm xc}^{\rm LDA}(n) + f_{\rm xc}^{\rm LDA}(n,t)\,. \tag{16}$$

In this, $\varepsilon_{\rm xc}^{\rm LDA}$ is the ground-state LDA XC energy per particle [49], $f_{\rm xc}^{\rm LDA}$ is the LDA XC free-energy per particle Eq. (3), and the PBE XC energy per particle is defined via the X enhancement factor, $F_{\rm x}^{\rm PBE}$, and C function H as

$$\varepsilon_{\rm xc}^{\rm PBE}(n,\nabla n) = \varepsilon_{\rm x}^{\rm LDA}(n) F_{\rm x}^{\rm PBE}(s^2) + \varepsilon_{\rm c}^{\rm LDA}(n) + H(\varepsilon_{\rm c}^{\rm LDA}, \mathcal{Q})\,. \tag{17}$$

In somewhat the same spirit, Kozlowski *et. al.* [24] proposed a "divide and multiply" scheme in which the ground-state PBE XC energy per particle is scaled by the thermal LDA XC. That gives what those authors called the locally thermal PBE (ltPBE) approximation

$$\begin{aligned} f_{\rm xc}^{\rm ltPBE}(n,s,t) &= \varepsilon_{\rm xc}^{\rm PBE}(n,\nabla n)\frac{f_{\rm xc}^{\rm LDA}(n,t)}{\varepsilon_{\rm xc}^{\rm LDA}(n)} \\ &\equiv \varepsilon_{\rm xc}^{\rm LDA}(n) F_{\rm xc}^{\rm ltPBE}(n,\nabla n,t)\,. \end{aligned} \tag{18}$$

In it, the LDA XC temperature dependence effectively is absorbed by the XC dimensionless enhancement factor

$$F_{\rm xc}^{\rm ltPBE}(n,\nabla n,t) := \frac{\varepsilon_{\rm xc}^{\rm PBE}(n,\nabla n)}{\varepsilon_{\rm xc}^{\rm LDA}(n)}\frac{f_{\rm xc}^{\rm LDA}(n,t)}{\varepsilon_{\rm xc}^{\rm LDA}(n)}\,. \tag{19}$$

So far as we are aware this scheme has not been tested on physically realistic systems; see our further discussion below.

Both the additive (addPBE) and multiplicative (ltPBE) schemes account for thermal XC corrections (relative to the ground state) only at the LDA level of refinement. Spatial inhomogeneity effects are described by the ground-state PBE gradient-dependent terms without any explicit T-dependence (the only T-dependent spatial gradient contributions are through the T-dependence of the density). Consequently neither scheme matches the second-order finite-T gradient expansion in the weakly varying density limit. That limit is important especially in the WDM regime. This seems to be the main disadvantage of such simplified schemes versus the fully thermal KDT16 GGA, See Ref. [50] for further details and see Sect. III for new results.

D. Meta-GGA: basics of ground-state approximation

The next theoretical refinement rung is meta-GGA XC functionals. They have additional functional variable information in the form of either dependence on the (Mermin)-Kohn-Sham kinetic energy density or upon the density Laplacian. Currently the most successful ground-state meta-GGA is the strongly constrained and appropriately normed (SCAN) functional. It is built to obey 17 exact constraints known to be relevant to meta-GGA XC functionals [51]. On most systems (though there are exceptions [52]), SCAN is much more accurate than GGA functionals for properties such as atomization energies, molecular bond lengths, barrier heights for chemical reactions, weak interaction energies (hydrogen and van der Waals bonds), and lattice constants of solids. SCAN has numerical instabilities however (*e.g.* numerical grid sensitivity, slow self-consistent field (SCF) convergence, some divergence issues) that have limited its utility for large-scale ground-state simulations. The recently proposed regularized-restored version of SCAN, r^{2}SCAN, improves the numerical performance and restores (largely) the transferable accuracy of SCAN [53, 54].

Like most conventional meta-GGAs, SCAN and r^{2}SCAN are explicitly orbital-dependent via the non-interacting kinetic energy density. As such they are useless for any orbital-free DFT (ofDFT) approach [50, 55]. As mentioned at the outset, replacement of that orbital dependence with dependence upon the reduced density Laplacian $q := \nabla^2 n/4(3\pi^2)^{2/3} n^{5/3}$ constitutes "de-orbitalization". The objective is to recover a pure Kohn-Sham (local) XC potential and, as well, to make a meta-GGA useful in ofDFT. For the ground-state SCAN and r^{2}SCAN functionals this has been explored in Refs. [56–58]. The de-orbitalized versions are denoted SCAN-L and r^{2}SCAN-L respectively.

E. Meta-GGA: GGA thermal corrected

The first version of thermalization of a ground-state meta-GGA XC functional was an additive correction scheme very much akin to addPBE discussed above; recall Eq. (16). Thus, Ref. 8 discussed strategies for thermalization of ground-state meta-GGA XC functionals, and implemented a simple but usefully accurate scheme via a universal additive thermal GGA-level correction. For virtually any meta-GGA ground-state XC functional, one defines a universal additive thermal GGA correction

$$\Delta\mathcal{F}_{\rm xc}^{\rm GGA}[n,T] = \mathcal{F}_{\rm xc}^{\rm KDT16}[n,T] - E_{\rm xc}^{\rm PBE}[n]\,. \tag{20}$$

This correction is combined with the selected meta-GGA ground-state XC to give the simple T-dependent meta-GGA, to wit

$$\mathcal{F}_{\rm xc}^{\rm meta-GGA}[n,{\rm T}] = E_{\rm xc}^{\rm meta-GGA}[n] + \Delta\mathcal{F}_{\rm xc}^{\rm GGA}[n,{\rm T}]\,. \tag{21}$$

The scheme was applied to the deorbitalized versions of SCAN and r^{2}SCAN, SCAN-L and r^{2}SCAN-L respectively, to yield thermal orbital-free T-SCAN-L and T-r^{2}SCAN-L meta-GGAs. Importantly, both of those functionals reduce very closely to the ground-state counterpart at low-T, and to the KDT16 GGA at high-T. Details are in Refs. 8, 50.

It is important to emphasize that this additive correction approach should not be used with the original SCAN and r^{2}SCAN functionals at least as they are implemented, for example, in the VASP package. Formally, both SCAN and r^{2}SCAN are ground-state functionals. However, the "iso-orbital indicator" which they use is

$$\alpha(n,\nabla n,\{\psi\}) := (t_{\rm s}-t_{\rm vW})/t_{\rm TF} \tag{22}$$

with

$$t_{\rm s} = \frac{1}{2}\sum_{i=1}^{N_{\rm e}} |\nabla\psi_i|^2 \tag{23}$$

being the KS kinetic energy density of $N_{\rm e}$ electrons in the ground state, and $t_{\rm vW}$ and $t_{\rm TF}$ the von Weizsäcker and Thomas-Fermi kinetic energy densities respectively. (Beware inescapable notational overload: plain t is reduced temperature.) Obviously this KE density also can be written with explicit Fermi-Dirac occupation numbers

$$\tau_{\rm s}^{\rm MKS}(\{\psi\},T) = \frac{1}{2}\sum_{i=1}^{\infty} f_i(T)|\nabla\psi_i|^2\,, \tag{24}$$

with the ground-state recovered by setting the $f_i(T)$ to $T=0$ integer values. At $T>0$, however, this latter implementation takes partial account of thermal XC effects (beyond those implicit in n and s). Use in conjunction with the additive $\Delta\mathcal{F}_{\rm xc}^{\rm GGA}$ thermal correction thus would lead, in general, to uncontrolled (and unevaluatable) double counting.

F. Meta-GGA: fully thermalized

To generate thermal counterparts of the orbital-dependent ground-state SCAN XC functional requires thermal extension of the iso-orbital indicator, $\alpha(n,\nabla n,\{\psi\})$, Eq. (22). The other dependencies are the GGA-level reduced density gradient s defined below Eq. (8), that appears in X and C terms. The ground-state s-dependencies are replaced by the T-dependent dimensionless gradients, $s_{2\rm x}$ Eq. (10), and $\mathcal{Q}_{\rm c}$ Eq. (11), in the X and C terms respectively.

An important step for appropriate thermalization of α is the recognition that its numerator is the zero-T Pauli KED, $t_\theta := t_{\rm s} - t_{\rm vW}$ encountered in ofDFT. It is known that $t_\theta \geq 0$. That non-negativity immediately constrains $\alpha \geq 0$. The modified Pauli KED defined at finite-T, $\tau_\theta(n,\nabla n,\{\psi\}) = \tau_{\rm s}^{\rm MKS} - t_{\rm vW}(n,\nabla n)$, also is strictly non-negative [59, 60]. Thus the T-dependent iso-orbital indicator that preserves the non-negativity property and reduces to the ground-state α is defined as

$$\alpha_T(n,\nabla n,\{\psi\}) := \frac{\tau_{\rm s}^{\rm MKS}(\{\psi\},T) - t_{\rm vW}(n,\nabla n)}{\tau_{\rm TF}(n,T)}\,. \tag{25}$$

The remaining tasks are to thermalize the ingredient functional (called h_1 in SCAN) which causes α_T switching in X and the corresponding objects in C. In X that is done in terms of s_{2x} defined at Eq. (10) and α_T as well as by modifying h_1 into $h_{\rm 1ftSCAN}^1$ in fully thermal SCAN (ftSCAN)). All of this is done in compliance with relevant gradient expansion terms more or less analogous with the development of the KDT16 GGA. The intricate details of the fully thermal fT(r^2) SCAN meta-GGA that results are in Ref. 9.

G. Thermal hybrid XC: global and range-separated

It is well known that semi-local XC density functionals yield HOMO-LUMO eigenvalue differences that underestimate the fundamental electronic band gap ($I-A$). This discrepancy is a consequence of omission of derivative discontinuity [61]. That is a fundamental issue in KS-DFT because of the local multiplicative XC potential (though there are work-arounds [62]). An improvement is offered by the development of density functionals with a non-local potential operator, such as an orbital-dependent meta-GGA, provided that the variational treatment is in generalized KS fashion [63]. The same is true of hybrid XC functionals, such as the PBE0 global hybrid [64, 65] and the HSE range-separated one [66]. They are constructed by combining an explicit density functional XC approximation (DFA) and a fraction of Fock (F) exchange (the non-local functional form arising in the Hartree-Fock approximation). The additional distinction is between use of the explicit Fock contribution for the full Coulomb interaction or a short-range part in the case of global and range-separated hybrids respectively.

Development of finite-T (thermal) versions of the PBE0 and HSE hybrids was presented in Refs. 25, 26. The thermal counterpart of the PBE0 global hybrid XC functional, KDT0 was constructed by mixing of the thermal Fock exchange, $\mathcal{F}_{\rm x}^{\rm F}[n,T]$, with the fully thermal GGA KDT16 exchange, $\mathcal{F}_{\rm x}^{\rm KDT16}[n,T]$. Correlation is treated entirely by the thermal KDT16 DFA. The result is

$$\mathcal{F}_{\rm xc}^{\rm KDT0}[n,T] = \mathcal{F}_{\rm xc}^{\rm KDT16}[n,T] + a(\mathcal{F}_{\rm x}^{\rm F}[n,T] - \mathcal{F}_{\rm x}^{\rm KDT16}[n,T])\,. \tag{26}$$

In this expression, a is the mixing parameter. It is set to $a=0.25$, similar to the ground-state PBE0 global hybrid. Thus, as $T\to 0$, thermal KDT0 reduces very

closely to the ground-state PBE0. As emphasized in our discussion of guiding principles for thermalization, such limiting behavior is required for any thermal XC DFA to be useful without inconsistencies across the entire range of real system T.

Although global hybrid functionals provide more accurate fundamental band gap values than LDA and GGA DFAs or meta-GGAs done in gKS, they overestimate small system gaps. That flaw, which also occurs in metallic systems, is due to screening effects which are missing from Fock exchange. Additionally, global hybrids are computationally expensive because of the long-range, non-local character of Fock exchange.

Range-separated HSE hybrid XC functionals tackle this issue by separating the exchange functional into long-range (LR) and short-range (SR) contributions. The mixing (hybridization) between the non-local and semi-local DFA forms is done only for the SR exchange components. The full DFA is used for the LR-exchange and correlation. The range-separated HSE generally provides better agreement with experiments than do the global hybrids [67, 68].

In the ground-state HSE functional, the range separation of the PBE X involves a rather complicated utilization of the PBE exchange hole density to compute the screened PBE exchange enhancement factor. The thermal version of HSE uses a simpler range-separation procedure for the DFA exchange. The screened Coulomb interaction is embedded in the fully thermal KDT16 X functional via the thermal LDA exchange term, and the full KDT16 exchange enhancement factor (compare to Eq. (12)), as follows

$$\mathcal{F}_{\rm x}^{\rm SR,\omega KDT16}[n,T] = \int n f_{\rm x}^{\rm SR,\omega LDA}(n,t) F_{\rm x}^{\rm KDT16}(s_{2\rm x}) {\rm d}\mathbf{r}\,. \tag{27}$$

In this ω is the usual Coulomb interaction screening parameter used for the construction of range-separated X terms,

$$\frac{1}{|\mathbf{r}-\mathbf{r}'|} = \frac{{\rm erfc}(\omega|\mathbf{r}-\mathbf{r}'|)}{|\mathbf{r}-\mathbf{r}'|} + \frac{{\rm erf}(\omega|\mathbf{r}-\mathbf{r}'|)}{|\mathbf{r}-\mathbf{r}'|}\,. \tag{28}$$

The LR contribution of the KDT16 exchange is calculated as a difference $\mathcal{F}_{\rm x}^{\rm LR,\omega KDT16}[n,T] = \mathcal{F}_{\rm x}^{\rm KDT16}[n,T] - \mathcal{F}_{\rm x}^{\rm SR,\omega KDT16}[n,T]$. Similarly with the ground-state HSE functional, the thermal range-separated RS-KDT0 functional mixes the SR thermal Fock exchange and SR thermal DFA exchange

$$\begin{aligned}\mathcal{F}_{\rm xc}^{\text{RS-KDT0}}[n,T] &= \mathcal{F}_{\rm xc}^{\rm KDT16}[n,T] \\ &+ a(\mathcal{F}_{\rm x}^{\rm SR,\omega F}[n,T] - \mathcal{F}_{\rm x}^{\rm SR,\omega KDT16}[n,T])\,.\end{aligned} \tag{29}$$

Further details on the construction of the thermal Fock and thermal LDA range-separated exchange free-energy can be found in Refs. 26, 69.

III. ASSESSING THE PERFORMANCE OF THERMAL XC FUNCTIONALS AT EXTREME AND NEAR-AMBIENT CONDITIONS

For assessment of the accuracy of thermal XC functionals in the challenging warm-dense regime, we performed a few sets of AIMD simulations for warm-dense H/D and He plasmas at thermodynamic conditions for which accurate reference path-integral Monte Carlo (PIMC) data are available and thermal XC effects are not negligible. Detailed description of computational details can be found in Refs. [9] and [70] for H/D and He respectively.

For the hydrogen/deuterium plasma, Table I gives comparative data for the total pressure along the $r_{\rm s} = 3.0$ isochore and along the $T = 62,500$ K isotherm. Results are from the KDT16 fully-thermal GGA, the LDA thermal-corrected approximate GGAs (ltPBE and addPBE), and both full thermal meta-GGA (fTSCAN) and the approximate one (T-r^{2}SCAN-L). Additionally, we performed corrKSDT thermal LDA simulations at a few selected conditions to provide additional perspective on the accuracy of the ltPBE and addPBE approximate thermal GGAs (see below).

The magnitude of *explicit* thermal XC effects can be characterized usefully by the relative pressure deviation of the results from the widely used ground-state PBE XC functional with respect to the PIMC reference values [16], specifically $100 \times (P^{\rm PBE} - P^{\rm PIMC})/P^{\rm PIMC}$. Table I shows that these *explicit* thermal effects range between 1.3% and 6.7% with a mean absolute value of 3.6%, reported in Table I as the mean absolute relative deviation (MARD) at the bottom of the PBE column. *All* of the thermal functionals with the GGA and meta-GGA level of thermalization have drastically reduced deviations. The reduction from KDT16 is a factor of nine (0.4%), from fTSCAN it is four (0.9%), and from T-r^{2}SCAN-L, six (0.6%).

Even the two LDA thermal-corrected GGAs, ltPBE and addPBE, improve on GSA PBE, but with larger errors than from the other three free-energy functionals, 1.7% and 1.8% respectively. That difference leads to comparison between the behavior of those two functionals and the corrKSDT thermal LDA. At least at selected conditions and for this specific system, Table I shows that the pure thermal LDA actually provides better accuracy than the thermal LDA-corrected GGAs. The corrKSDT LDA MARD value reduces to 1.5%, as compared to 1.7% and 1.8% for the ltPBE and addPBE functionals respectively.

This very interesting finding has gone unnoticed before. It demonstrates that ground-state reduced density X and C gradients (i.e. gradients without explicit temperature dependence) can be inconsistent with LDA thermal corrections, hence *can decrease* accuracy relative to a pure thermal LDA treatment. It is unclear what thermodynamic conditions and/or system ingredients lead to this inconsistency. Hence it also is unclear how to avoid the inconsistency in actual calculations.

The contrast with the full thermal GGA performance demonstrates that consistent inclusion of reduced density gradients with explicit T-dependence, is required for significant improvement in accuracy compared to thermal LDA. (As an aside, we emphasize that at very high T the thermal XC effects will be of negligible magnitude, and essentially independent on the XC functional choice. Recall discussion of Fig. 2).

Table II shows results for He plasmas along two isotherms for the same set of XC functionals but with SCAN-L added (another example of the ground-state approximation). The PBE MARD (relative to PIMC reference values [17]) is almost identical to the H/D case, 3.7%. The MARD of the ground-state SCAN-L meta-GGA MARD decreases modestly to 3.1%. In contrast, use of KDT16, fTSCAN, and T-SCAN-L thermal XC functionals reduces MARD values to below 1%. As in the case of the H/D plasmas just discussed, the LDA thermal-corrected ltPBE and addPBE GGA functionals yield substantially larger errors, 2.4% and 2.5% respectively. Comparison of ltPBE or addPBE results with pure thermal LDA values confirms the interesting (and unappreciated before now) feature that LDA thermal-corrected GGAs are less accurate than the corrKSDT LDA. The ltPBE and addPBE MARD values of 2.4% and 2.5% respectively, are reduced to 1.8% for the corrKSDT LDA. Recall discussion just above.

Fully thermal GGA and thermal meta-GGAs, as Tables I and II show, provide very similar accuracy with respect to the PIMC reference data. This is expected at the elevated temperatures considered here, as the effects of density gradients and Laplacians diminish as T increases (because densities become smoother).

However, it also is expected that meta-GGA functionals should be more accurate than the KDT16 GGA at lower temperatures. Figure 3 provides one demonstration of the point. That figure compares the pressure-volume cold curves (300 K) of MgO in the B1 phase, calculated with a variety of XC functionals, with experimental values [71]. LDA XC underestimates the pressure. The PBE and KDT16 GGA curves are atop each other as they should be since KDT16 essentially reduces to PBE at low-T. Both give pressure overestimates. All the meta-GGA functionals represented in that Figure reproduce the experimental data well, though ground-state SCAN slightly underestimates the pressure. The PBEsol GGA was developed specifically for use with solids, with the expected result that the PBEsol curve also is very accurate. Figure 3 also illustrates the first of our fundamental principles, namely that a thermal XC functional must reduce to a well-founded ground-state counterpart in the $T \to 0$ limit. Thus KDT16 reduces to PBE, T-SCAN-L reduces to SCAN-L, and fTSCAN reduces quite closely to ground-state SCAN.

Now we present illuminating results obtained with hybrid XC functionals. Hybrids, both global and range-separated, are still too computationally costly to perform routine, large-system AIMD simulations. A conse-

TABLE I. Comparison of total pressure values (in Mbar) for warm dense deuterium/hydrogen from PIMC reference data [16] and as computed using the ground-state PBE (GGA) and the free-energy KDT16, fTSCAN, T-r^{2}SCAN-L, addPBE and ltPBE XC functionals. Relative deviations with respect to the PIMC reference are given in parentheses. Thermal LDA (corrKSDT) results for selected conditions also are shown for comparison. Mean absolute relative deviation (MARD), defined as the average of the absolute values of relative deviations $|P^{\rm DFA} - P^{\rm PIMC}|/P^{\rm PIMC} \times 100\%$ for each functional is reported in the last line.

T (kK)	r_s	t	PIMC	PBE	KDT16	fTSCAN	T-r^{2}SCAN-L	ltPBE	addPBE	corrKSDT
62.5	2.6	0.73	1.044	1.0976 (+5.1)	1.0432 (-0.1)	1.0451 (+0.1)	1.0330 (-1.1)	1.0706 (+2.5)	1.0714 (+2.6)	1.0663 (+2.1)
	3.5	1.32	0.4343	0.4527 (+4.4)	0.4359 (+0.3)	0.4390 (+1.1)	0.4322 (-0.5)	0.4436 (+2.1)	0.4441 (+2.3)	0.4429 (+2.0)
	4.0	1.72	0.29689	0.30811 (+3.8)	0.29840 (+0.5)	0.30099 (+1.4)	0.29651 (-0.1)	0.30254 (+1.9)	0.30301 (+2.1)	0.30227 (+1.8)
	4.5	2.18	0.21366	0.21970 (+2.8)	0.21448 (+0.4)	0.21685 (+1.5)	0.21348 (-0.1)	0.21649 (+1.3)	0.21656 (+1.4)	0.21647 (+1.3)
	5.0	2.67	0.1592	0.16268 (+2.2)	0.15993 (+0.5)	0.16138 (+1.4)	0.15930 (+0.06)	0.16075 (+1.0)	0.16071 (+0.9)	0.16085 (+1.0)
50.0	3.0	0.77	0.5005	0.5338 (+6.7)	0.5036 (+0.6)	0.5030 (+0.5)	0.4957 (-1.0)	0.5206 (+4.0)	0.5225 (+4.4)	0.5172 (+3.3)
62.5		0.97	0.6901	0.7121 (+3.2)	0.6805 (-1.4)	0.6840 (-0.9)	0.6719 (+2.6)	0.6971 (+1.0)	0.6970 (+1.0)	0.6944 (+0.6)
75.0		1.16	0.8659	0.8995 (+3.9)	0.8660 (+0.01)	0.8727 (+0.8)	0.8600 (+0.7)	0.8802 (+1.7)	0.8814 (+1.8)	0.8789 (+1.5)
95.25		1.47	1.17896	1.21113 (+2.7)	1.18194 (+0.3)	1.1908 (+1.0)	1.17771 (-0.1)	1.19113 (+1.0)	1.19194 (+1.1)	1.19200 (+1.1)
125.0		1.93	1.6652	1.6869 (+1.3)	1.6652 (-0.0)	1.6763 (+0.7)	1.6649 (-0.02)	1.6691 (+0.2)	1.6703 (+0.3)	1.6701 (+0.3)
MARD(%)	-	-	-	3.6	0.4	0.9	0.6	1.7	1.8	1.5

TABLE II. Comparison of total pressure data (in Mbar) for warm dense helium from PIMC reference calculations [17] and as computed using the ground-state PBE (GGA) and SCAN-L (meta-GGA) functionals versus the free-energy KDT16, fTSCAN, T-SCAN-L, addPBE and ltPBE XC functionals. Relative deviations with respect to the PIMC reference are given in parentheses. Thermal LDA (corrKSDT) results for selected conditions are also shown for comparison. Mean absolute relative deviation (MARD), defined as the average of the absolute values of relative deviations $|P^{\mathrm{DFA}} - P^{\mathrm{PIMC}}|/P^{\mathrm{PIMC}} \times 100\%$ for each functional is reported in the last line.

T (kK)	r_s	t	PIMC	PBE	SCAN-L	KDT16	fTSCAN	T-SCAN-L	ltPBE	addPBE	corrKSDT
125.0	2.4	0.66	1.723	1.797 (+4.3)	1.786 (+3.7)	1.741 (+1.0)	1.739 (+0.9)	1.728 (+0.3)	1.769 (+2.7)	1.771 (+2.8)	1.763 (+2.3)
	2.2	0.86	2.239	2.329 (+4.0)	2.312 (+3.3)	2.248 (+0.4)	2.251 (+0.5)	2.240 (+0.04)	2.298 (+2.6)	2.300 (+2.7)	2.278(+1.7)
	2.0	1.04	2.974	3.127 (+5.1)	3.099 (+4.2)	3.007 (+1.1)	2.999 (+0.8)	2.985 (+0.4)	3.070 (+3.2)	3.079 (+3.5)	3.045 (+2.4)
	1.75	1.24	4.544	4.807 (+5.8)	4.740 (+4.3)	4.606 (+1.4)	4.560 (+0.4)	4.550 (+0.1)	4.701 (+3.5)	4.695 (+3.3)	4.658 (+2.5)
250.0	2.4	1.32	4.457	4.522 (+1.5)	4.515 (+1.3)	4.488 (+0.7)	4.507 (+1.1)	4.485 (+0.6)	4.505 (+1.1)	4.507 (+1.1)	4.501 (+1.0)
	2.2	1.72	5.696	5.816 (+2.1)	5.803 (+1.9)	5.748 (+0.9)	5.767 (+1.2)	5.743 (+0.8)	5.789 (+1.6)	5.786 (+1.6)	5.774 (+1.4)
	2.0	2.08	7.459	7.671 (+2.8)	7.649 (+2.5)	7.552 (+1.2)	7.568 (+1.5)	7.537 (+1.0)	7.608 (+2.0)	7.615 (+2.1)	7.595 (+1.8)
	1.75	2.48	10.980	11.371 (+3.6)	11.331 (+3.2)	11.146 (+1.5)	11.180 (+1.8)	11.089 (+1.0)	11.250 (+2.5)	11.261 (+2.6)	11.217 (+2.2)
MARD(%)	-	-	-	3.7	3.1	1.0	1.0	0.5	2.4	2.5	1.8

quence is that it is common for such functionals to be employed for band gap predictions of static structures at low-T or band gap and transport property calculations of solid/liquid structures at elevated temperatures. Typically the static calculations are for a set of so-called snapshot ion configurations along an AIMD trajectory driven by a lower-rung XC functional calculation .

Thus, to illustrate the performance of thermal hybrid XC functionals under extreme thermodynamic conditions, we computed band gaps for Si and CH_4 at elevated electronic temperatures. Computational details are provided in Ref. [26]. The ionic positions were fixed for both materials. For Si the lattice constants are from HSE calculations in Ref. [72], while those for CH_4 are from Ref. [25]. Only the electronic temperature was varied. That singles out the explicit thermal contributions of the XC functional. Physically, this computational scenario is relevant to pump–probe experiments [73, 74]. In them, an intense ultrashort laser pulse drives the electrons to high temperatures on sub-picosecond time scales, while the ions remain effectively cold. This leads to a non-equilibrium regime accompanied by a reduction in the band gap as the electronic temperature increases.

Figure 4(a) shows the band-gap results for Si, a representative semiconductor. At low T, RS-KDT0 converges to the HSE06 value. Both agree well with the experimental band gap (indicated by the golden star). In contrast, the GGA-level XC functionals PBE and KDT16 both underestimate the gap by approximately 50%. Moreover, PBE and KDT16 incorrectly predict an increasing gap with increasing electronic temperature. On the other hand, KDT0, RS-KDT0, and HSE06 all show band-gaps decreasing with increasing T, in agreement with finite-temperature GW (FT-GW) results [75]. RS-KDT0 provides the closest agreement. We note that the HSE06 results employ a thermal SR-HF exchange but use a zero-temperature GGA component. That includes only partial thermal effects. Similar trends are observed in other small-band-gap materials, further confirmation of the importance of including explicit thermal XC effects [26].

As an example of a wide-band-gap system, Fig. 4(b) shows the results for calculations on CH_4. Overall, thermal hybrid XC functionals predict consistently larger band gaps than thermal GGA-level functionals. PBE exhibits approximately linear increase with temperature, while KDT16 is convex with a minimum at $T \approx 15$ kK. That corresponds to comparatively strong thermal corrections to GGA XC that weaken again at higher temperature. The HSE06 band gap remains nearly constant for $T < 40$ kK, showing that the thermal SR-HF exchange largely counteracts the temperature dependence of the GGA part. At low temperatures ($T < 15$ kK), the band-gap trends of RS-KDT0 and KDT0 are dominated by the thermal GGA contributions, similar to KDT16, followed by a saturation at higher temperatures. Rather little seems to be known about the direct gap in crystalline CH_4 but an early correlation-corrected Hartree-Fock calculation [76] gave 13.3 eV. A newer LDA calculation [77]

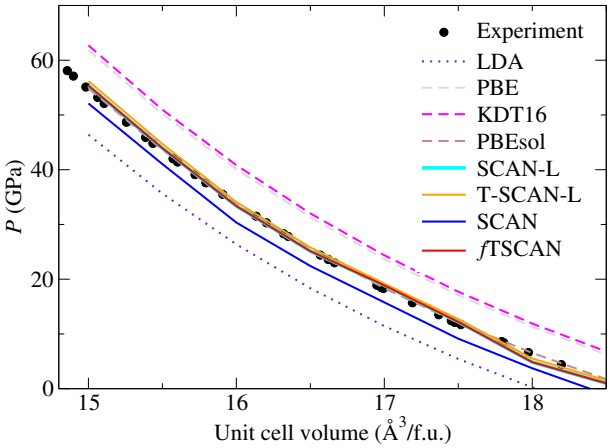

FIG. 3. Comparison of cold curves for MgO in the B1 phase as computed with a variety of XC functionals versus experimental data [71] (black points). Meta-GGA functionals, ground-state and thermalized versions, SCAN-L, T-SCAN-L, SCAN and *f*TSCAN (solid curves), along with the GGA PBEsol functional greatly outperform the remaining GGA (PBE and KDT16 (dashed curves) and LDA (dotted curve) functionals.

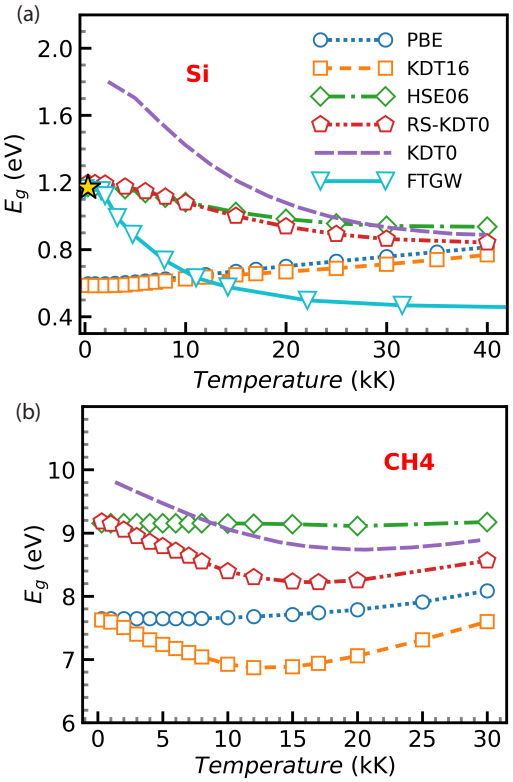

FIG. 4. Band-gap calculations for static structures as a function of electronic temperature. (a) Results for Si, shown as an example of a small-band-gap material; the gold star indicates the experimental band gap at low temperature. (b) Results for CH_4, representing a wide-band-gap material. Two panels are reproduced from Ref. [26].

gives about 7.7 eV, but LDA is known to underestimate gaps by 40-50%. The results shown in Fig. 4(b) are consistent with this. Both PBE and KDT16 give about 7.7 eV for the $T = 0$ gap, while the KDT0 gap extrapolates to roughly 10 eV at $T = 0$.

IV. CONCLUSIONS

The most important elements of constraint-based development of thermal XC functionals on four rungs of increasing complexity, LDA, GGA, meta-GGA (including fully thermal versions) and hybrids, have been summarized. As a basic design principle, all thermal XC functionals reduce closely to well-founded ground-state counterparts. Thus, the thermal functionals inherit, for better or worse, the essential properties of those counterparts latter ones. Thus the thermal versions can be used safely across the entire range of temperatures associated with non-ideal plasmas, warm dense matter, etc.

For the benefit of possible users, we have assessed the accuracy of currently available thermal functionals by performing AIMD simulations of dense H/D and He plasmas and comparing results to PIMC reference data. Fully thermal GGA and meta-GGA provide near-identical accuracy. That is expected for sufficiently elevated temperatures. Importantly, those functionals outperform LDA thermal-corrected GGAs (ltPBE and addPBE). An important new result is that thermal corrKSDT LDA can outperform the LDA thermal-corrected GGAs. This demonstrates the uncontrolled risk in using ground-state-corrected functionals. One does not know under what circumstances they succeed or fail. It also illustrates the importance of reduced density gradients that have explicit, correct temperature dependence for the development of accurate thermal functionals. Such gradients are absent in ltPBE and addPBE, Thermal hybrids exhibit the correct qualitative behavior of band gaps for static structures with an increase in temperature. However, the range separated RS-KDT0 hybrid provides more reliable predictions as compared to the global KDT0 one.

ACKNOWLEDGMENTS

This work is supported by the U.S. Department of Energy (National Nuclear Security Administration), University of Rochester "National Inertial Confinement Fusion Program" under Award No. DE-NA0004144, and U.S. National Science Foundation PHY Grant No. 2020249.

This report was prepared as an account of work sponsored by an agency of the U.S. Government. Neither the U.S. Government nor any agency thereof, nor any of their employees, makes any warranty, express or implied, for the accuracy, completeness, or usefulness of any

DATA AVAILABILITY

The data that support the findings of this study are available from the corresponding author upon reasonable request.

[1] W. Kohn and L. J. Sham, Self-consistent equations including exchange and correlation effects, Phys. Rev. **140**, A1133 (1965).

[2] N. D. Mermin, Thermal properties of the inhomogeneous electron gas, Phys. Rev. **137**, A1441 (1965).

[3] T. Dornheim, P. Tolias, F. Kalkavouras, Z. A. Moldabekov, and J. Vorberger, Dynamic exchange correlation effects in the strongly coupled electron liquid, Phys. Rev. B **110**, 075137 (2024).

[4] V. V. Karasiev, L. Calderín, and S. B. Trickey, Importance of finite-temperature exchange correlation for warm dense matter calculations, Phys. Rev. E **93**, 063207 (2016).

[5] V. V. Karasiev, J. W. Dufty, and S. B. Trickey, Nonempirical semilocal free-energy density functional for matter under extreme conditions, Phys. Rev. Lett. **120**, 076401 (2018).

[6] V. V. Karasiev, S. X. Hu, M. Zaghoo, and T. R. Boehly, Exchange-correlation thermal effects in shocked deuterium: Softening the principal hugoniot and thermophysical properties, Phys. Rev. B **99**, 214110 (2019).

[7] K. Ramakrishna, T. Dornheim, and J. Vorberger, Influence of finite temperature exchange-correlation effects in hydrogen, Phys. Rev. B **101**, 195129 (2020).

[8] V. V. Karasiev, D. I. Mihaylov, and S. X. Hu, Meta-gga exchange-correlation free energy density functional to increase the accuracy of warm dense matter simulations, Phys. Rev. B **105**, L081109 (2022).

[9] K. P. Hilleke, V. V. Karasiev, S. B. Trickey, R. M. N. Goshadze, and S. X. Hu, Fully thermal meta-gga exchange correlation free-energy density functional, Phys. Rev. Mater. **9**, L050801 (2025).

[10] M. Bonitz, J. Vorberger, M. Bethkenhagen, M. P. Böhme, D. M. Ceperley, A. Filinov, T. Gawne, F. Graziani, G. Gregori, P. Hamann, S. B. Hansen, M. Holzmann, S. X. Hu, H. Kählert, V. V. Karasiev, U. Kleinschmidt, L. Kordts, C. Makait, B. Militzer, Z. A. Moldabekov, C. Pierleoni, M. Preising, K. Ramakrishna, R. Redmer, S. Schwalbe, P. Svensson, and T. Dornheim, Toward first principles-based simulations of dense hydrogen, Physics of Plasmas **31**, 110501 (2024).

[11] M. Bogojeski, L. Vogt-Maranto, M. E. Tuckerman, K.-R. Müller, and K. Burke, Quantum chemical accuracy from density functional approximations via machine learning, Nature Commun. **11**, 5223 (2020).

[12] G. Fabbro, J. Brandjes, and T. Saue, Highly accurate expectation values using high-order relativistic coupled cluster theory, J. Phys. Chem. A **129**, 6942 (2025).

[13] J. C. Smith, A. Pribram-Jones, and K. Burke, Exact thermal density functional theory for a model system: Correlation components and the accuracy of the zero-temperture exchange-correlation approximation, Physical Review B **93**, 245131 (2016).

[14] S. X. Hu, B. Militzer, V. N. Goncharov, and S. Skupsky, First-principles equation-of-state table of deuterium for inertial confinement fusion applications, Phys. Rev. B **84**, 224109 (2011).

[15] S. X. Hu, B. Militzer, V. N. Goncharov, and S. Skupsky, Strong coupling and degeneracy effects in inertial confinement fusion implosions, Phys. Rev. Lett. **104**, 235003 (2010).

[16] A. V. Filinov and M. Bonitz, Equation of state of partially ionized hydrogen and deuterium plasma revisited, Phys. Rev. E **108**, 055212 (2023).

[17] B. Militzer, Path integral monte carlo and density functional molecular dynamics simulations of hot, dense helium, Phys. Rev. B **79**, 155105 (2009).

[18] J. P. Perdew and K. Schmidt, Jacob's ladder of density functional approximations for the exchange-correlation energy, AIP Conf. Proc. **577**, 1 (2001).

[19] V. V. Karasiev, T. Sjostrom, J. Dufty, and S. B. Trickey, Accurate homogeneous electron gas exchange-correlation free energy for local spin-density calculations, Phys. Rev. Lett. **112**, 076403 (2014).

[20] S. Groth, T. Dornheim, T. Sjostrom, F. D. Malone, W. M. C. Foulkes, and M. Bonitz, Ab initio exchange-correlation free energy of the uniform electron gas at warm dense matter conditions, Phys. Rev. Lett. **119**, 135001 (2017).

[21] E. W. Brown, B. K. Clark, J. L. DuBois, and D. M. Ceperley, Path-integral monte carlo simulation of the warm dense homogeneous electron gas, Phys. Rev. Lett. **110**, 146405 (2013).

[22] T. Dornheim, S. Groth, T. Sjostrom, F. D. Malone, W. M. C. Foulkes, and M. Bonitz, Ab initio quantum monte carlo simulation of the warm dense electron gas in the thermodynamic limit, Phys. Rev. Lett. **117**, 156403 (2016).

[23] T. Sjostrom and J. Daligault, Gradient corrections to the exchange-correlation free energy, Phys. Rev. B **90**, 155109 (2014).

[24] J. Kozlowski, D. Perchak, and K. Burke, Generalized gradient approximation made thermal, arXiv:2308.03319v2 10.48550/arXiv.2308.03319 (2023).

[25] D. I. Mihaylov, V. V. Karasiev, and S. X. Hu, Thermal hybrid exchange-correlation density functional for improving the description of warm dense matter, Phys. Rev. B **101**, 245141 (2020).

[26] A. A. Ellaboudy, V. V. Karasiev, D. I. Mihaylov, K. P. Hilleke, and S. X. Hu, Range-separated thermal hy-

brid exchange-correlation density functional for accurate band-gap calculations of warm dense matter, Phys. Rev. B **00**, 00 (2025).
[27] J. W. Dufty and S. B. Trickey, Finite temperature scaling in density functional theory, Mol. Phys. **114**, 988 (2016).
[28] J. P. Perdew and A. Zunger, Self-interaction correction to density-functional approximations for many-electron systems, Phys. Rev. B **23**, 5048 (1981).
[29] D. M. Ceperley and B. J. Alder, Ground state of the electron gas by a stochastic method, Phys. Rev. Lett. **45**, 566 (1980).
[30] R. P. Feynman, N. Metropolis, and E. Teller, Equations of state of elements based on the generalized fermi-thomas theory, Phys. Rev. **75**, 1561 (1949).
[31] V. V. Karasiev, T. Sjostrom, and S. B. Trickey, Generalized-gradient-approximation noninteracting free-energy functionals for orbital-free density functional calculations, Phys. Rev. B **86**, 115101 (2012).
[32] G. A. Baker and J. L. Gammel, eds., *The Pade Approximant in Theoretical Physics,* (Academic Press, NY, 1970).
[33] S. Ichimaru, Nuclear fusion in dense plasmas, Reviews of Modern Physics **65**, 255 (1993).
[34] T. Schoof, S. Groth, J. Vorberger, and M. Bonitz, Ab initio thermodynamic results for the degenerate electron gas at finite temperature, Phys. Rev. Lett. **115**, 130402 (2015).
[35] V. V. Karasiev, S. B. Trickey, and J. W. Dufty, Status of free-energy representations for the homogeneous electron gas, Phys. Rev. B **99**, 195134 (2019).
[36] F. Perrot, Gradient correction to the statistical electronic free energy at nonzero temperatures: Application to equation-of-state calculations, Phys. Rev. A **20**, 586 (1979).
[37] J. Bartel, M. Brack, and M. Durand, Extended thomas-fermi theory at finite temperature, Nuclear Physics A **445**, 263 (1985).
[38] P. Hohenberg and W. Kohn, Inhomogeneous electron gas, Phys. Rev. **136**, B864 (1964).
[39] E. Dunlap and D. J. W. Geldart, Nonlocal exchange contribution to the free energy of inhomogeneous many–fermion systems. i: Formulation of the gradient expansion, Canadian Journal of Physics **72**, 1 (1994).
[40] M. L. Glasser, D. J. W. Geldart, and E. Dunlap, Nonlocal exchange contribution to the free energy of inhomogeneous many-fermion systems. ii: Second-order gradient coefficient for a coulomb system, Canadian Journal of Physics **72**, 7 (1994).
[41] M. R. A. Shegelski, D. J. W. Geldart, M. L. Glasser, and D. Neilson, Nonlocal exchange contribution to the free energy of inhomogeneous many-fermion systems. iii: Numerical study for screened coulomb interaction, Canadian Journal of Physics **72**, 14 (1994).
[42] D. J. W. Geldart, Nonlocal energy functions: Gradient expansions and beyond, in *Density Functional Theory I: Functionals and Effective Potentials*, edited by R. F. Nalewajski (Springer Berlin Heidelberg, Berlin, Heidelberg, 1996) pp. 31–55.
[43] G. Niklasson, A. Sjölander, and K. S. Singwi, Exchange and correlation in the electron gas, Phys. Rev. B **11**, 113 (1975).
[44] A. K. Gupta and K. S. Singwi, Gradient corrections to the exchange-correlation energy of electrons at metal surfaces, Phys. Rev. B **15**, 1801 (1977).
[45] V. V. Karasiev, D. Chakraborty, and S. Trickey, Improved analytical representation of combinations of fermi–dirac integrals for finite-temperature density functional calculations, Computer Physics Communications **192**, 114 (2015).
[46] J. P. Perdew, K. Burke, and M. Ernzerhof, Generalized gradient approximation made simple, Physical review letters **77**, 3865 (1996).
[47] E. H. Lieb and S. Oxford, Improved lower bound on the indirect coulomb energy, International Journal of Quantum Chemistry **19**.
[48] S. Pittalis, C. R. Proetto, A. Floris, A. Sanna, C. Bersier, K. Burke, and E. K. U. Gross, Exact conditions in finite-temperature density-functional theory, Phys. Rev. Lett. **107**, 163001 (2011).
[49] J. P. Perdew and Y. Wang, Accurate and simple analytic representation of the electron-gas correlation energy, Phys. Rev. B **45**, 13244 (1992).
[50] V. Karasiev, K. Hilleke, and S. Trickey, Free-energy OFDFT: Recent developments, perspective, and outlook, Electr. Struct. **7**, 013001 (2025).
[51] J. Sun, A. Ruzsinszky, and J. P. Perdew, Strongly constrained and appropriately normed semilocal densiy functioi nal, Physical Review Letters **115**, 036402 (2015).
[52] D. Mejía-Rodríguez and S. B. Trickey, Analysis of overmagnetization of elemental transition metal solids from the scan density functional, Physical Review B **100**, 041113(R) (2019).
[53] A. P. Bartók and J. R. Yates, Regularized scan functional, The Journal of Chemical Physics **150**, 161101 (2019).
[54] J. W. Furness, A. D. Kaplan, J. Ning, J. P. Perdew, and J. Sun, Accurate and numerically efficient r2scan meta-generalized gradient approximation, The Journal of Physical Chemistry Letters **11**, 8208 (2020), pMID: 32876454.
[55] W. Mi, K. Luo, S. Trickey, and M. Pavanello, Orbital-free density functional theory: An attractive electronic structure method for large-scale first-principles simulations, Chemical Reviews **123**, 12039 (2023).
[56] D. Mejía-Rodríguez and S. B. Trickey, Deorbitalization strategies for meta-generalized-gradient-approximation exchange-correlation functionals, Phys. Rev. A **96**, 052512 (2017).
[57] D. Mejía-Rodríguez and S. B. Trickey, Deorbitalized meta-gga exchange-correlation functionals in solids, Phys. Rev. B **98**, 115161 (2018).
[58] D. Mejía-Rodríguez and S. B. Trickey, Meta-gga performance in solids at almost gga cost, Phys. Rev. B **102**, 121109 (2020).
[59] J. W. Dufty and S. B. Trickey, Scaling, bounds, and inequalities for the noninteracting density functionals at finite temperature, Phys. Rev. B **84**, 125118 (2011).
[60] R. M. N. Goshadze, V. V. Karasiev, K. P. Hilleke, and S. X. Hu, Pauli potential formalism at finite temperature, Phys. Rev. B **111**, 235143 (2025).
[61] J. P. Perdew and M. Levy, Physical content of the exact kohn-sham orbital energies: Band gaps and derivative discontinuities, Phys. Rev. Lett. **51**, 1884 (1983).
[62] J. Carmona-Espíndola, J. Gázquez, A. Vela, and S. Trickey, Generalized gradient approximation exchange functional with near-best-semilocal performance, Journal of Chemical Theory and Computation **15**, 303 (2019).

[63] Z.-h. Yang, H. Peng, J.-w. Sun, and J. P. Pedew, More realistic band gaps from meta-generalized gradient approximations; only in a generalized kohn-sham scheme, Phys. Rev. B , 205205 (2016).

[64] J. P. Perdew, M. Ernzerhof, and K. Burke, Rationale for mixing exact exchange with density functional approximations, The Journal of Chemical Physics **105**, 9982 (1996).

[65] C. Adamo and V. Barone, Toward reliable density functional methods without adjustable parameters: The pbe0 model, The Journal of Chemical Physics **110**, 6158 (1999).

[66] J. Heyd, G. E. Scuseria, and M. Ernzerhof, Hybrid functionals based on a screened coulomb potential, The Journal of Chemical Physics **118**, 8207 (2003).

[67] J. P. Perdew, W. Yang, K. Burke, Z. Yang, E. K. U. Gross, M. Scheffler, G. E. Scuseria, T. M. Henderson, I. Y. Zhang, A. Ruzsinszky, H. Peng, J. Sun, E. Trushin, and A. Görling, Understanding band gaps of solids in generalized kohn–sham theory, Proceedings of the National Academy of Sciences **114**, 2801 (2017).

[68] M. Marsman, J. Paier, A. Stroppa, and G. Kresse, Hybrid functionals applied to extended systems, Journal of Physics: Condensed Matter **20**, 064201 (2008).

[69] F. Xuan, J.-D. Chai, and H. Su, Local density approximation for the short-range exchange free energy functional, ACS omega **4**, 7675 (2019), pMID: 31459859.

[70] V. V. Karasiev, J. Hinz, and R. M. N. Goshadze, Framework for laplacian-level noninteracting free-energy density functionals, The Journal of Physical Chemistry Letters **15**, 8272 (2024).

[71] S. D. Jacobsen, C. M. Holl, K. A. Adams, R. A. Fischer, E. S. Martin, C. R. Bina, J.-F. Lin, V. B. Prakapenka, A. Kubo, and P. Dera, Compression of single-crystal magnesium oxide to 118 gpa and a ruby pressure gauge for helium pressure media, American Mineralogist **93**, 1823 (2008).

[72] J. Heyd, J. E. Peralta, G. E. Scuseria, and R. L. Martin, Energy band gaps and lattice parameters evaluated with the heyd-scuseria-ernzerhof screened hybrid functional, The Journal of Chemical Physics **123**, 174101 (2005).

[73] A. J. Sabbah and D. M. Riffe, Femtosecond pump-probe reflectivity study of silicon carrier dynamics, Phys. Rev. B **66**, 165217 (2002).

[74] L. Huang, J. P. Callan, E. N. Glezer, and E. Mazur, Gaas under intense ultrafast excitation: Response of the dielectric function, Phys. Rev. Lett. **80**, 185 (1998).

[75] S. V. Faleev, M. van Schilfgaarde, T. Kotani, F. m. c. Léonard, and M. P. Desjarlais, Finite-temperature quasiparticle self-consistent GW approximation, Phys. Rev. B **74**, 033101 (2006).

[76] A. B. Kunz, Electronic structure and optical properties of solid methane, Physical Review B **28**, 3465 (1983).

[77] H. Lin, Y.-l. Li, Z. Zeng, X.-j. Chen, and H. Q. Lin, Structural, electronic, and dynamical properties of methane under high pressure, J. Chem. Phys. **134**, 064515 (2011).